Proceedings of the Combustion Institute 41 (2025) 105856

Contents lists available at ScienceDirect

Proceedings of the Combustion Institute

journal homepage: www.elsevier.com/locate/proci

Influence of dispersion length on volume-averaged simulations of ammonia/air combustion in porous media burners

Rishabh Puri [a,*], Daniel Kretzler [a], Benjamin Bock-Seefeld [c], Björn Stelzner [a], Nora Brachhold [c], Jana Hubálková [c], Dimosthenis Trimis [a], Christos Aneziris [c], Oliver T. Stein [a], Thorsten Zirwes [b]

[a] KIT- Karlsruhe Institute of Technology, Engler-Bunte-Institute, Combustion Technology, Engler-Bunte Ring 7, D-76131 Karlsruhe, Germany
[b] University of Stuttgart, Institute for Reactive Flows, Pfaffenwaldring 31, D-70569 Stuttgart, Germany
[c] TU Bergakademie Freiberg, Institute of Ceramics, Refractories and Composites, Agricolastraße 17, D-09599 Freiberg, Germany

ARTICLE INFO

Keywords:
Porous media combustion
Volume-averaged simulations
Ammonia combustion

ABSTRACT

Ammonia is a carbon-free alternative to fossil fuels and can potentially be integrated in the existing energy infrastructure. However, due to poor flame stability and high pollutant emissions, clean combustion of ammonia is a current topic of research. Porous media burners have shown potential to improve the combustion characteristics of ammonia and ammonia blends, which are otherwise difficult to stabilise in conventional burners. Combustion in porous media can be investigated in great detail by performing three-dimensional direct pore-level simulations (3D-DPLS). However, 3D-DPLS with complex ammonia chemistry are computationally expensive. Volume-averaged simulations (VAS) are an efficient alternative for numerical investigations of porous burners. In this work, a comprehensive VAS framework is proposed for 1D, 2D, and 3D transient VAS, taking variable porosity, detailed chemistry and diffusion into account. The numerical framework allows for on-the-fly definitions of constitutive models for effective properties, e.g. tortuosity, dispersion and permeability. After successful validation with other VAS cases from literature, the new code is used to analyse an experimentally investigated novel porous ammonia burner. The analysis is performed to study the effect of the characteristic dispersion length of the solid matrix, which is hard to measure for practical geometries, on pollutant formation and energy balance. All other effective properties are obtained directly from μ-CT scans. Both fuel-lean and fuel-rich conditions of ammonia/air combustion in porous media are investigated. As the characteristic dispersion length increases, local peak temperatures decrease. This significantly affects the predicted NO_x and NH_3 emissions. Higher dispersion lengths lead to a broadening of the flame zone that can lead to larger lift-off heights from the burner inlet and merging of neighbouring flames Therefore, reliable estimates of characteristic dispersion lengths are required to achieve good predictions from VAS.

1. Introduction

Today's combustion processes are driven by the goal of increasing efficiency and minimising pollutant emissions. The desire to achieve a net zero carbon economy has made the combustion of alternative fuels a highly relevant topic for research [1,2]. Although carbon-free fuels such as hydrogen provide a potential solution to clean energy supply, the low volumetric density of H_2 renders its transport and storage difficult [3]. On the other hand, ammonia, which can be produced from hydrogen, can easily be liquefied for transport and storage in the current energy infrastructure [4]. However, NH_3 exhibits poor combustion characteristics in conventional burners due to its low heating value and high pollutant emissions [5–7].

Porous media combustion (PMC) can be utilised to improve the combustion characteristics of NH_3 [8–10]. PMC refers to combustion of a gaseous mixture within a solid matrix, which allows the fuel and oxidiser to flow through the cavities of a porous structure. The flame inside the pores heats up the solid structure, which in turn transports heat to the upstream regions by means of conduction in the solid and thermal radiation. [11]. This heat transfer within the solid matrix and heat re-circulation to the upstream fuel/oxidiser mixture can improve the flame stability of NH_3. The physics governing PMC are an interplay of flow dispersion within the solid matrix, complex chemical kinetics, conjugate, and radiative heat transfer. These physical phenomena can be investigated numerically by performing direct pore-level simulations

* Corresponding author.
E-mail address: rishabh.puri@kit.edu (R. Puri).

https://doi.org/10.1016/j.proci.2025.105856
Received 2 May 2025; Accepted 5 September 2025
Available online 20 September 2025

(DPLS) [12–14], where all length and time scales associated with the physical and chemical phenomena need to be resolved. This restriction on the resolution of the computational grid as well as the complex chemistry of NH_3 combustion lead to very high computational costs. Therefore, a viable numerical approach is required to investigate different burner operating conditions and multiple configurations of porous structures with varying geometric and material properties.

A popular numerical approach for large-scale porous media burners is volume-averaged simulation (VAS) in which the solid matrix is not resolved. Instead, the properties of both the solid and gas phase are averaged within a control volume and coupled through inter-phase heat transfer. Closure models are required to describe the effective geometric and material properties of the averaged phases. To model complex and interdependent phenomena of flow dispersion and inter-phase heat transfer within the porous structure, accurate calculations of effective parameters for the solid matrix need to be performed. Attempts have been made to define correlations and models for the effective material properties as well as to analyse their effects on VAS predictions. Sathe et al. [15] investigated a porous radiant burner using a 1D model and a one-step global mechanism. High inter-phase heat transfer ensured local thermal equilibrium, and low solid heat conductivity and scattering albedo were found to increase the radiation efficiency. Hsu et al. [16] performed simulations of combustion in porous media with multi-step chemical kinetics and found that higher convective heat transfer and effective thermal conductivity of the solid led to stronger preheating in the porous burner.

Reduced VAS models have also been implemented for multi-zone porous burners. Barra et el. [11] conducted a parameter study for a two-zone porous burner and proposed different properties for individual porous zones to achieve stable operation of the burner. The variation in temperature and species concentrations for different operating conditions, pore size, and extinction coefficients was investigated by Mishra et al. [17] for combustion of CH_4-air in a two-zone porous burner. Sahraoui at al. [18] compared results of VAS with that of 2D-DPLS for CH_4-air combustion and found that VAS with thermal non-equilibrium (two-media) yielded better results compared to VAS with a single-medium treatment, where local thermal equilibrium between solid and gas was assumed. Bidi et al. [19] presented detailed modelling of the solid matrix for a 2D-VAS and analysed the flame stabilisation of a submerged flame in porous media by the entropy generation minimisation (EGM) method.

VAS models defined using empirical correlations for the effective properties have shown higher discrepancies with DPLS and experiments. A detailed determination of the geometric properties (pore size, specific surface area, porosity. etc.) of the porous structures can be made by X-ray micro-computed-tomography (μ-CT). Heat transfer properties can be estimated by performing thermal simulations using the solid geometry obtained from μ-CT [20,21]. Zirwes et al. [22] developed a steady-state 1D-VAS solver in the framework of Cantera [23] for multi-zone porous media combustion and utilised μ-CT scans to obtain the topology of different porous structures. The evaluated material effective properties were validated for an interface-stabilised NH_3-H_2-air combustion burner. Masset et al. [12] investigated the influence of porous topology obtained from X-ray tomography on volume-averaged modelling and used DPLS to calculate macroscopic material properties.

While most effective properties of the porous structure can be derived from μ-CT scans, reliable evaluation of the characteristic dispersion length still poses challenges. Most of the above-mentioned approaches did not include dispersion modelling. One of the early attempts was made by Henneke and Ellzey [24], who defined dispersion coefficients as functions of Peclet number for 1D simulations of CH_4-air combustion in a packed bed and found that dispersion only affected combustion at high equivalence ratios. Parthasarathy et al. [25] determined the characteristic dispersion length by following an initial tracer jump in non-reactive DPLS of air flow in open-cell foams. This definition of the dispersion length was used by Bedoya et al. [26] to implement a 1D-VAS for natural gas combustion. The increased burning velocity in PMC was attributed to the heat and mass dispersion in the porous medium. The effect of dispersion on PMC was also investigated by Hsu [27]. Dispersion was integrated in a 1D model using correlations for mass and thermal dispersion in the energy equation. Masset et al. [12] determined hydrodynamic dispersion from a steady-state isothermal non-reactive simulation and found that dispersion plays an important role in heat transfer within the gas phase. However, the above-mentioned VAS, when compared with DPLS, still have discrepancies in spatially-averaged temperature profiles [12,26].

In this work, a comprehensive VAS framework is presented which enables full flexibility in terms of porous structures and operating conditions. The model allows for multi-zone solid matrices, where the properties of each zone can be configured individually and impromptu. A two-media treatment that omits the assumption of thermal equilibrium is implemented by solving separate but coupled energy equations for the gas and the solid phases. With this numerical framework, an experimentally investigated porous media burner, operated with ammonia, is characterised using VAS. The focus is put on quantifying the effect of dispersion length modelling on overall flame characteristics.

The manuscript is structured as follows: in Section 2, the numerical methods of the new VAS model are described and the implementation of closure models is presented. In Section 3, the VAS model is validated against several reference cases and in Section 4, the effect of dispersion modelling in VAS of the experimentally investigated porous media burner for ammonia/air combustion is analysed. Finally, the findings are summarised, conclusions are drawn, and an outlook is given in Section 5.

2. Numerical methods

The OpenFOAM-based transient reacting flow solver EBIdnsFoam [28] is used as the basis for the development of the new VAS framework. The VAS solver computes molecular properties with Cantera [23], considers variable porosity and closure models for the solid phase (tortuosity, dispersion, Rosseland radiation). Direct integration of Cantera routines into the solver reduces external dependence. The solver also supports accurate thermodiffusion and the mixture-averaged transport model for H_2-based fuels. The governing equations are written for the volume-averaged variables $\bar{\bar{\theta}}$, which are defined as

$$\bar{\bar{\theta}}_g = \frac{1}{\mathcal{V}_g}\int_{\mathcal{V}_g} \theta \,\mathrm{d}V \quad \text{and} \quad \bar{\bar{\theta}}_s = \frac{1}{\mathcal{V}_s}\int_{\mathcal{V}_s} \theta \,\mathrm{d}V \tag{1}$$

where the subscripts g and s denote the gas and solid phase, respectively. For simplicity, the variables in the following governing equations are written without the averaging ($\bar{\bar{}}$) notation and properties without subscript denote the properties of the gas phase.

The continuity and momentum equations in the volume-averaged form are

$$\frac{\partial(\gamma\rho)}{\partial t} + \nabla\cdot(\gamma\rho\vec{u}) = 0 \tag{2}$$

$$\frac{\partial(\gamma\rho\vec{u})}{\partial t} + \nabla\cdot(\gamma\rho\vec{u}\vec{u}) = -\gamma\nabla p + \nabla\cdot(\gamma\boldsymbol{\tau}) + \gamma\rho\vec{g} - \vec{u}_{\mathrm{sup}}\left(\frac{\mu}{k_1} + \frac{\rho}{k_2}|\vec{u}_{\mathrm{sup}}|\right) \tag{3}$$

where $\vec{u}$ is the interstitial gas velocity, ρ the density, p the pressure, $\vec{g}$ the gravitational acceleration, γ is the porosity, and $\vec{u}_{\mathrm{sup}} = \gamma\vec{u}$ is the superficial velocity. The last term on the RHS of Eq. (3) is the Darcy–Forchheimer term for pressure loss due to flow through the porous material. k_1 and k_2 are the linear and turbulent permeability coefficients, respectively. The above form of the mass and momentum conservation equation with variable porosity is based on the spatially-averaged formulation [29] of the volume-averaged equations. The shear stress tensor is defined as

$$\boldsymbol{\tau} = \mu\left(\nabla\vec{u} + (\nabla\vec{u})^T - \frac{2}{3}\mathbf{I}\nabla\cdot\vec{u}\right) \tag{4}$$

where **I** is the identity tensor and μ is the viscosity.

To consider the effect of heat transfer from the solid structure, the energy equation for the gas phase can be written in terms of total sensible enthalpy as

$$0 = \underbrace{-\frac{\partial(\gamma\rho h_{\mathrm{tot}})}{\partial t}}_{\text{transient}} \underbrace{-\nabla\cdot(\gamma\rho\vec{u}h_{\mathrm{tot}})}_{\text{convection}} \underbrace{-\nabla\cdot(\gamma\vec{q})}_{\text{heat flux}} + \underbrace{\gamma\frac{\partial p}{\partial t}}_{\text{pressure derivative}} \underbrace{-\gamma\sum_k(h_k^0\dot{\omega}_k)}_{\text{chemistry}} - \underbrace{h_v(T-T_s)}_{\text{inter-phase heat transfer}} \tag{5}$$

where h_v is the heat transfer coefficient and the total sensible energy is $h_{\mathrm{tot}} = h_{\mathrm{sens}} + \frac{1}{2}\vec{u}\cdot\vec{u}$, with the sensible enthalpy h_{sens}. Eq. (5) accounts for flow dispersion by the solid matrix and heat flux reads,

$$\vec{q} = \underbrace{-(D_{\mathrm{disp}}\rho)\nabla h_{\mathrm{sens}}}_{\text{dispersion}} + \underbrace{\sum_k h_{\mathrm{sens},k}\hat{\vec{j}}_k}_{\text{differential diffusion}} + \underbrace{\frac{\lambda}{c_p\eta}\left(-\nabla h_{\mathrm{sens}} + \sum_k h_{\mathrm{sens},k}\nabla Y_k\right)}_{\text{Fourier}} \tag{6}$$

where λ is the thermal conductivity of the gas, c_p the isobaric heat capacity, η the tortuosity, k the index of the kth species, $h_{\mathrm{sens},k}$ the sensible enthalpy of species k and $\hat{\vec{j}}_k = \vec{j}_k - Y_k\sum_k\vec{j}_k$ the conservative molecular diffusive species flux. Dispersion is considered in the VAS energy equation in the form of an additional diffusion term to model the unresolved inter-phase heat transfer between the gas and the solid matrix. The dispersion coefficient is calculated using the correlation of DeMaria and White [30] as,

$$D_{\mathrm{disp}} = \frac{1}{2}|\vec{u}|d_{\mathrm{disp}} \tag{7}$$

where d_{disp} is the characteristic dispersion length. The gas species conservation equation reads

$$\frac{\partial(\gamma\rho Y_k)}{\partial t} + \nabla\cdot(\gamma\rho(\vec{u}+\vec{u}_c)Y_k) = \gamma\dot{\omega}_k - \nabla\cdot(\gamma\vec{j}_k) \tag{8}$$

where Y_k is the mass fraction, $\dot{\omega}_k$ the reaction rate of species k, and $\vec{j}_k$ the diffusive flux. The correction velocity is given by $\vec{u}_c = -\frac{1}{\rho}\sum_k\vec{j}_k$. The diffusive fluxes are expressed as:

$$\vec{j}_k = \vec{j}_k^{\mathrm{mass}} + \vec{j}_k^{\mathrm{thermo}} \tag{9}$$

Thermodiffusion [31] is calculated from

$$\vec{j}_k^{\mathrm{thermo}} = -\frac{D_k^T}{\eta T}\nabla T, \tag{10}$$

where D_k^T is the thermodiffusion coefficient of species k. The diffusive mass flux for the VAS model is computed as

$$\vec{j}_k^{\mathrm{mass}} = -\rho\left(\frac{D_{m,k}^{\mathrm{mole}}}{\eta} + D_{\mathrm{disp}}\right)\nabla Y_k - Y_k\rho\frac{D_{m,k}^{\mathrm{mole}}}{\bar{M}\eta}\nabla\bar{M} \tag{11}$$

where $\bar{M}$ is the mean molar mass of the mixture, and the diffusion coefficient is

$$D_{m,k}^{\mathrm{mole}} = \frac{1-Y_k}{\sum_{j\neq k}\frac{X_j}{D_{j,k}}} \tag{12}$$

where X_j is the mole fraction and $D_{j,k}$ the binary diffusion coefficient.

The energy equation for the solid phase reads

$$0 = \underbrace{-(1-\gamma)\rho_s c_s\beta\frac{\partial T_s}{\partial t}}_{\text{transient}} + \underbrace{\nabla\cdot(\lambda_{s,\mathrm{eff}}\nabla T_s)}_{\text{conduction}} + \underbrace{\nabla\cdot(\lambda_{\mathrm{rad}}\nabla T_s)}_{\text{radiation}} + \underbrace{h_v(T-T_s)}_{\text{inter-phase heat transfer}} \tag{13}$$

Table 1
Geometric and material properties of the YZA and SiC foams. d_p: mean pore diameter.

Property (unit)	YZA	SiC 3 PPI	SiC 10 PPI
γ (%)	82.5	86.2	86.0
d_p (mm)	1.11	1.56	1.07
S_v ($\mathrm{m^{-1}}$)	1,592	934	986
η (–)	1.34	1.17	1.15
a ($\mathrm{W\,m^{-1}\,K^{-1}}$)	0.38	4.62	3.95
b (–)	−0.35	−0.53	−0.53

where c_s is the heat capacity of the solid and the numerical coefficient β accelerates convergence to the steady state. The heat conductivity of the solid phase is $\lambda_{s,\mathrm{tot}} = \lambda_{s,\mathrm{eff}} + \lambda_{\mathrm{rad}}$, where $\lambda_{s,\mathrm{eff}}$ is the effective thermal conductivity of the solid and λ_{rad} is the radiative heat transfer using the Rosseland model [32] as $\lambda_{\mathrm{rad}} = 16\sigma T_s^3/(3\kappa)$, with σ the Stefan–Boltzmann constant and κ the extinction coefficient.

3. Validation

The new VAS framework is validated against other VAS cases from the literature. The closure models for the respective reference cases are updated impromptu in the VAS solver according to the models used in the literature. Further validation was performed with analytical solutions for non-reacting flow in porous media, radiation boundary condition for the solid phase and a pure-gas phase freely propagating flame, which are omitted here for brevity.

3.1. 1D-VAS: PMCToolBox

1D-VAS of H_2-air combustion in a four-zone burner were performed using the steady-state 1D-VAS solver PMCToolBox [22]. The porous zones are made of silicon carbide (SiC) and yttria-stabilised zirconia alumina (YZA) foams with a thickness of 25.4 mm. The SiC foams are characterised using the industrial designation *pores per inch* (PPI). The geometric and material properties of the solids are given in Table 1. Given the absence of dispersion modelling in PMCToolBox, dispersion due to the solid matrix is neglected in this section. The Darcy–Forchheimer pressure loss is also considered to be negligible.

The effective thermal conductivity $\lambda_{s,\mathrm{eff}}$ and heat transfer coefficient h_v for all zones are calculated as

$$\lambda_{s,eff} = a\left(\frac{T_s}{T_0}\right)^b, \qquad h_v = Nu\frac{S_v\lambda}{d_h} \tag{14}$$

where $T_0 = 293$K, $d_h = 4\gamma/S_v$ is the hydraulic diameter of the porous medium, S_v the specific surface area, and $Nu = 3.7Re^{0.38}Pr^{0.25}$ is the Nusselt number. The coefficients a and b are given in Table 1 and the Reynolds Re and Prandtl Pr numbers are

$$Re = \frac{\rho|\vec{u}|d_h}{\mu}, \qquad Pr = \frac{c_p\mu}{\lambda}. \tag{15}$$

VAS of H_2-air combustion at equivalence ratio $\phi = 0.9$ are performed with the mechanism by Li et al. [33]. At the inlet, constant mass flux ($\dot{m}_{\mathrm{in}} = 0.9$ kg $\mathrm{s^{-1}m^{-2}}$) and temperature ($T_{\mathrm{in}} = 300$ K) are imposed. The outlet is adiabatic and radiative heat transfer in the solid matrix is not considered ($\lambda_{\mathrm{rad}} = 0$). Considering the pressure–velocity coupling in Eqs. (2) and (3) and to validate the variable porosity implementation of the solver, VAS are investigated with both constant and variable porosity. In the first case, porosity is constant over the burner length ($\gamma = 0.86$) and the comparison with the PMCToolBox is shown in Fig. 1. In a second simulation, the porosity changes in each section according to Table 1. Results are compared to data from the PMCToolBox in Fig. 2 and excellent agreement is found for both cases.

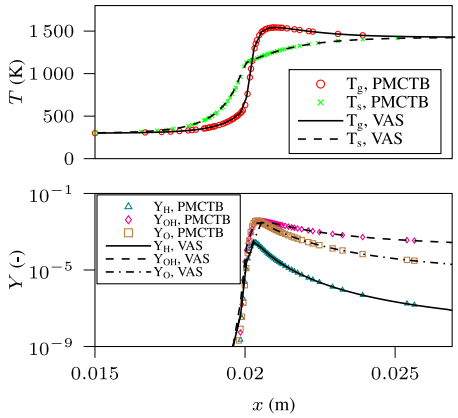

Fig. 1. VAS vs. PMCToolBox (PMCTB) for $\gamma = 0.86$. (top) temperatures, (bottom) species profiles.

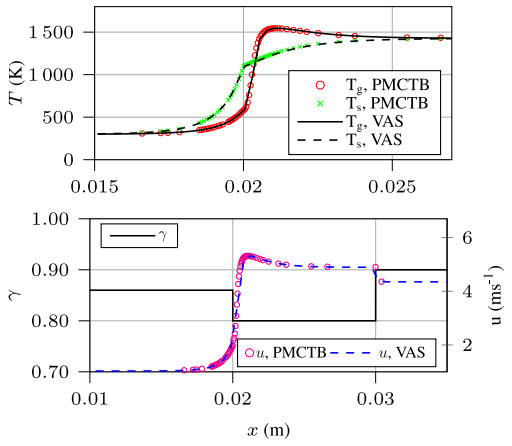

Fig. 2. VAS vs. PMCToolBox (PMCTB) for variable porosity. (a) Temperature, (b) Interstitial velocity.

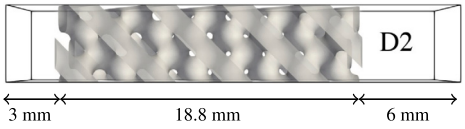

Fig. 3. Diamond triply-periodic minimal surface [12]. The CH_4-air mixture enters the domain from the left.

3.2. 1D-VAS: TPMS-D2

The effect of the geometry of the porous structure on the PMC of CH_4-air mixtures at $\phi = 0.72$ was investigated in [12], where the effective material properties were derived from DPLS. VAS for one of the investigated geometries from [12], a triply-periodic minimal surface diamond referred to here as TPMS-D2, is performed to further validate our VAS model.

The burner shown in Fig. 3 has three zones: (a) Upstream pure gas, (b) porous medium, and (c) downstream pure gas. For this validation case, only the first two zones are simulated. The effective material properties of the porous medium are given in Table 2. The property units are taken from [34].

Constant velocity ($u_{in} = 0.6$ m s^{-1}) and temperature ($T_{in} = 300$ K) at the inlet and an adiabatic outlet are imposed as boundary conditions. VAS is performed with the skeletal mechanism (CH4_24_148_0_AP) [35] with 24 species and 148 reversible reactions, whereas the Analytically-Reduced Chemistry (ARC) mechanism (CH4_15_138_9_AP) with 9 quasi

Table 2
Geometric and material properties of TPMS-D2.

Property (unit)	Value
γ (%)	62
d_p (mm)	2.02
η (–)	1
$\lambda_{s,eff}$ (W m^{-1} K^{-1})	1.7
d_{disp} (m)	6.2×10^{-4}
h_v (W m^2 K^{-1})	23×10^4

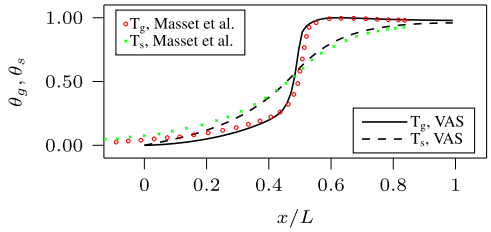

Fig. 4. VAS validation with data from Masset et al. [12].

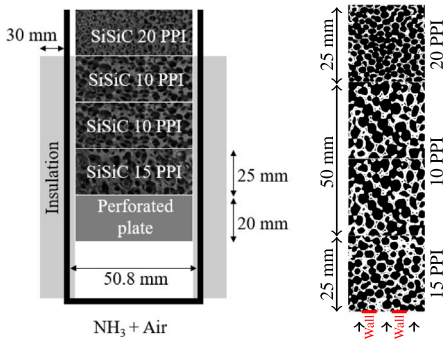

Fig. 5. Experimental setup of a porous media burner for NH_3-air combustion (left). Images of porous structures from μ-CT scans (right). The voxel size is 39 μm. The ratio of the wall area to the total inlet area is identical to the blockage ratio of the perforated plate used in the experiment. SiSiC: silicon infused silicon carbide.

steady-state species was used in the original work of Masset et al. [12]. The temperature profiles from the VAS and the original case are presented in Fig. 4, which show overall very good agreement.

4. NH_3 -air combustion in porous inert media

Given the scarcity of literature on VAS of NH_3-air combustion, the above code validation was performed for fuels other than ammonia. Here, we perform an *a posteriori* analysis of a porous media burner for ammonia-air combustion, which was experimentally investigated at KIT, see Fig. 5 (left). The three porous zones are arranged to ensure complete combustion of NH_3 and reduce emissions. Gas analysers (ABB) are used to measure the composition of the major exhaust gas species at the burner outlet. Uniform exhaust-gas distribution across the outflow diameter was confirmed, with deviations below 5%. The manufacturer specifies measurement uncertainties below 1.5%. N_2O is measured in the dehydrated gas phase, while NH_3, NO_x are measured in the wet gas phase to avoid losses due to condensation. Given that the burner inlet is defined by a perforated plate for homogeneous gas distribution, 2D-VAS are performed to account for the blockage ratio and diameter of the perforations. The numerical setup of the burner with three porous zones is shown in Fig. 5 (right). The NH_3-air mixture enters the burner from below and the width of the outer inlets is 1.6 times the central inlet.

Table 3
Parameters from X-ray μ-CT.

Parameter (unit)	Value
X-ray voltage (kV)	150
X-ray current (μA)	70
Voxel size (μm)	39
Scan size (voxels)	1600 × 1380 × 624

Table 4
Geometric and effective material properties used in the burner configuration for NH_3-air combustion.

Property (unit)	15 PPI	10 PPI	20 PPI
γ (%)	72.9	76.9	75.1
d_p (mm)	2.85	3.34	2.38
S_v (m^{-1})	891	714	1075
η (–)	1.48	1.31	1.45
a (W m^{-1} K^{-1})	10.4	8.18	8.02
κ (m^{-1})	650	525	831

Table 5
Inlet boundary conditions for NH_3-air combustion.

ϕ	$\dot{m}_{in}$ (kg s^{-1} m^{-2})	Re_{in} (–)	T_{in} (K)
0.9	2.6	271	1430
1.1	2.374	230	1418

The effective properties of the porous zones are calculated from μ-CT scans on a CT-ALPHA X-ray scanner (ProCon X-ray, Germany) with a Dexela Type 1512 (Perkin Elmer, Germany) detector. The operation parameters for μ-CT are summarised in Table 3.

All effective properties of the different porous zones were obtained from the scans using the open-source code PUMA. Only the dispersion length cannot be determined readily. Therefore, the contribution of this parameter to individual terms in the energy balance and pollutant formation is investigated in the next sections. Background noise in the scans is eliminated using a 3D Gaussian filter and the threshold values for segmentation into gas and solid phases are calculated using the Otsu method [36]. The coefficient a for the effective thermal conductivity in the axial direction and the tortuosity are calculated using a finite volume solver [21]. The extinction coefficients (κ) are derived from ray casting radiation simulations. The material properties of the individual zones are given in Table 4.

Coefficients $\lambda_{s,\mathrm{eff}}$ and h_v are calculated using the expressions defined in Eq. (14) with b = -0.53. The chemistry of NH_3-air combustion is calculated using the kinetic mechanism by Stagni et al. [37]. VAS are performed for a fuel-lean condition at $\phi = 0.9$ and a fuel-rich condition at ϕ = 1.1. The boundary conditions are based on the measurements and given in Table 5.

For the gas phase, the end of the domain is an outlet and gradients of velocity, temperature and species are set to zero at this boundary. A radiation loss boundary towards ambient temperature is imposed on the solid phase outlet. Periodic boundaries are implemented on the burner surfaces normal to the flow direction. The computational domain is uniformly discretised with a cell size of 1.25×10^{-4} m and has a total of 73,600 cells. A base value for d_{disp} is defined using the characteristic pore diameter d_p from the μ-CT scans as $\vartheta = d_{\mathrm{disp}}/d_p = 1$ and variations of d_{disp} around this value are investigated next.

4.1. Flame structure

The variation in d_{disp} strongly affects the structure of the NH_3-air flame. The flame structure at the fuel-lean condition (ϕ = 0.9) is compared for different d_{disp} in Fig. 6 and visualised through the OH mass fraction (left) and the chemical heat release rate $\dot{Q}$ (right). Note that only the upstream section starting from the perforated plate of the porous burner in Fig. 5 (right) is shown in Fig. 6. The reaction fronts

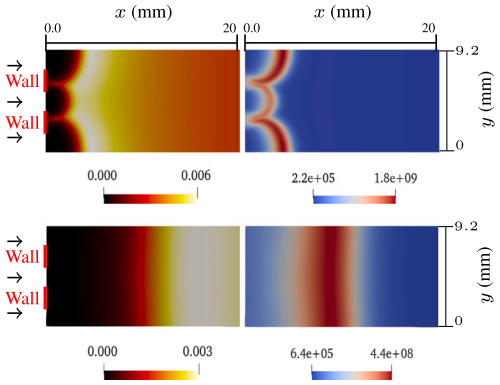

Fig. 6. Flame structure variation with ϑ, with ϑ = 1.0 (top row) and ϑ = 10.0 (bottom row) for ϕ = 0.9. Left: OH mass fraction (–), right: heat release rate (J m^{-3} s^{-1}).

are all located in the 15 PPI section of the burner. The total momentum through the central inlet is lower due to the smaller inlet area, leading to flames with higher power density at the top and bottom of this periodic section as observed at ϑ = 1.0. Species from the centre diffuse to the flame fronts at the top/bottom due to the enhanced diffusion, resulting in a broadening of the flame and a thinner flame at the centre. Predictably, the flame thickness increases with d_{disp} (Fig. 6, bottom row). This leads to the reaction zone lifting off from the inlet and a lifted, uniformly distributed flame front is observed for ϑ = 10.0. It is also important to consider the absolute values of the investigated quantities. For ϑ = 1.0, the peak OH mass fraction is twice the peak value at ϑ = 10.0. Similarly, the maximum $\dot{Q}$ is one order of magnitude higher for ϑ = 1.0 when compared with ϑ = 10.0.

4.2. Energy budget

The variations of selected individual terms in Eqs. (5),(6) and (13) with ϑ along the burner axis are shown in Fig. 7 for ϕ = 0.9. As already observed in Fig. 6, the reaction zone moves downstream for higher ϑ. Moreover, the reduction of peak values with increasing ϑ found in Fig. 6 is confirmed for the individual budget terms in Fig. 7. With increasing d_{disp}, the contribution of the peak dispersion term reduces by 35% to 2.37×10^8 J m^{-2} s^{-1} for ϑ = 10.0. There is a 52% reduction in differential diffusion with increasing ϑ, but its net contribution to energy transfer in the gas phase for respective ϑ is negligible compared to dispersion.

For higher ϑ, the peaks of the heat transfer terms in Eq. (13) also show a downstream movement and coincide with the reaction zone in the gas phase. The increased dispersion length leads to significant reduction in the inter-phase heat transfer (IHT), where the maximum value of IHT reduces by 85% to 3.2×10^7 J m^{-3} s^{-1} at ϑ = 10.0. This in turn leads to reduced conduction and radiation within the solid phase for higher ϑ.

4.3. Emissions

One important aspect for studying ammonia combustion in porous media burners is the reliable prediction of emission characteristics. Here, the variation of emissions with ϑ are shown in Fig. 8 and compared with experimental measurements. With increasing ϑ, i.e. increasing dispersion, the reaction zone of the flame broadens according to $\delta \propto \sqrt{D_{\mathrm{eff}}}$. Generally, the peak gas temperature $T_{g,\max}$ (black) decreases with increasing d_{disp}, resulting in lower NO_x emissions (blue) at fuel-lean conditions. On the other hand, NH_3 slip (non-pyrolised NH_3, red) at fuel-rich conditions is observed to increase with decreasing $T_{g,\max}$. For ϕ = 0.9, NO_x decreases for $\vartheta > 1.0$ and has a value of 1000 ppmv compared to experimentally measured 1092 ppmv at

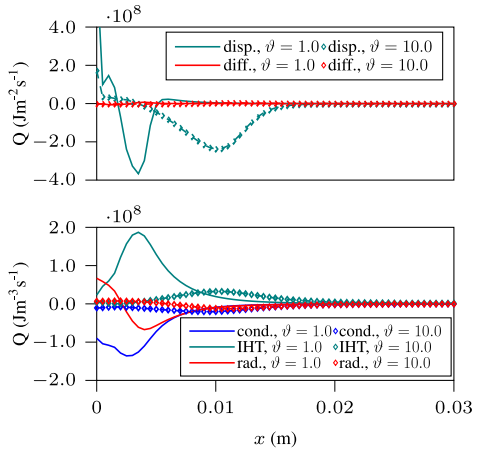

Fig. 7. Effect of d_{disp} on selected terms in the energy equations for gas (top) and solid (bottom) phase at $\phi = 0.9$. Gas energy balance, Eqs. (5),(6): disp.: dispersion, diff.: differential diffusion. Solid energy balance, Eq. (13): cond.: conduction, IHT: inter-phase heat transfer, rad.: radiation. (For interpretation of the references to colour in this figure legend, the reader is referred to the web version of this article.)

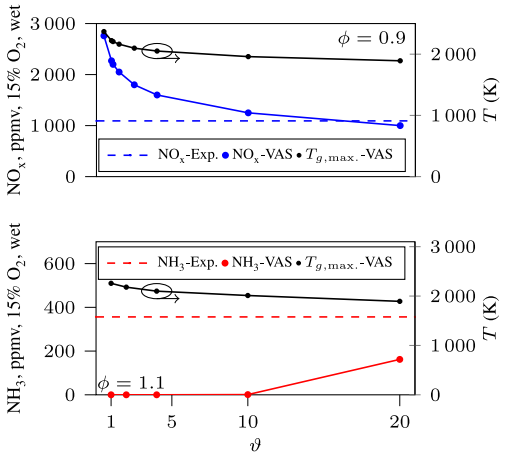

Fig. 8. VAS of NH_3-air combustion comparing peak gas temperatures, NO_x emissions at $\phi = 0.9$ (top) and unburnt ammonia emissions at $\phi = 1.1$ (bottom), performed for different characteristic dispersion lengths. Measured emissions are compared with the VAS results. (For interpretation of the references to colour in this figure legend, the reader is referred to the web version of this article.)

$\vartheta = 20.0$, which can be considered as good agreement considering the uncertainties in the VAS modelling approach. NO_x is negligible for $\phi = 1.1$ and therefore not shown, but a considerable NH_3 slip is calculated, which increases with ϑ. At $\vartheta = 20$, the predicted NH_3 slip is 162 ppmv against a measured value of 356 ppmv. It should be considered that higher NH_3 emissions in the experiment are expected, due to ammonia slip from imperfections in the experimental setup, compared to the perfectly homogenised burner in the VAS approach. N_2O (omitted for brevity) exhibits similar trends for both fuel conditions and has minimal variation for $1.0 \leq \vartheta \leq 20.0$. Therefore, $\vartheta \approx 20$ can be considered as a good estimate for dispersion in the given burner setup. It also shows that for ammonia combustion in porous media, dispersion modelling in VAS plays an important role for reliable emission predictions.

The variation in the VAS prediction is also investigated for uncertainty in the calculation of $\lambda_{\text{s,eff}}$. For this analysis, $\vartheta = 10$ and the coefficient a in Eq. (14) is replaced with $a' = \mathcal{K}a$. Finite volume thermal simulations are performed using PUMA [21] to calculate the coefficient

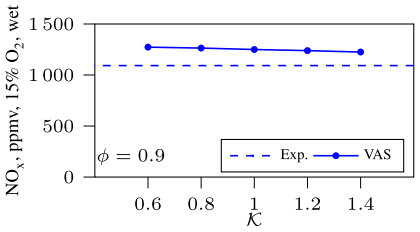

Fig. 9. Variation in VAS-predicted NO_x with $\lambda_{\text{s,eff}}$ for NH_3-air combustion at $\phi = 0.9$.

a and the factor $\mathcal{K}$ scales the effective thermal conductivities of each porous layer equally. The predicted NO_x emissions are plotted against the variation of $\mathcal{K}$ in Fig. 9. The total variation in NO_x for $0.6 \leq \mathcal{K} \leq 1.4$ is 48 ppmv. Hence, the VAS predictions show a slight sensitivity to variations of the calculated $\lambda_{\text{s,eff}}$, but the sensitivity of VAS with a fixed d_{disp} to such variations is negligible.

5. Conclusion and outlook

In this work, a comprehensive framework for performing volume-averaged simulations of combustion in porous media was presented. The model allows for impromptu updates of the closure models for the solid matrix and heat transfer, making it easily adaptable to different types of multi-zone porous structures. The model was validated against VAS cases from the literature, and the effect of characteristic dispersion length was investigated for an experimentally investigated NH_3-air porous media burner. The following conclusions can be drawn from this work: VAS of H_2-air combustion in a three-zone porous burner were in good agreement with the results from the Cantera-based PMCToolbox [22] as well as for CH_4-air combustion in a TPMS porous burner. The flame position predicted by VAS closely matched the literature data, showing that the new modelling framework gives reliable predictions for porous media flames.

For the experimentally investigated burner, variation in d_{disp} has shown a strong influence on the flame structure. An increase in d_{disp} increases the flame thickness, which can lead to the flame lifting from the inlet plate of the porous media burner. At the same time, peak chemical heat release rate and thus peak gas-phase temperatures are lowered as well. Increasing d_{disp} leads to a downstream movement of the reaction zone and a net reduction in the peaks of the individual budget terms in the gas and solid energy equations.

With increasing dispersion length, NO_x emissions decreased for the lean flame and unburnt NH_3 emissions increased for the rich flame, both as a consequence of the lower peak temperatures. A characteristic dispersion length of 20 times the pore diameter (d_{disp}) showed good agreement with the experimental results, while values lower than $10d_{\text{disp}}$ show signifiant deviations. This highlights the importance of good approximations for dispersion lengths in order to ensure accurate emission predictions from VAS. The emissions predicted by the VAS framework were in good agreement with the experimental results for the selected operating conditions. However, the spatial variation of the material properties in a porous foam was not considered in the VAS framework, limiting its generalisability. Investigation of the applicability of the VAS model to other operating conditions will be the focus of future work.

Novelty and significance statement

The novelty of this work is the analysis of dispersion length modelling for volume-averaged simulations (VAS) of ammonia/air combustion in porous media. VAS using state-of-the-art closure models are performed using a comprehensive numerical modelling framework, which allows for on-the-fly updates of closure models for the effective

properties of the porous medium. The dispersion length, which is hard to measure in practical geometries, is varied as a function of the mean pore diameter and combustion characteristics are evaluated for both fuel-lean and fuel-rich conditions. The results provide crucial insights into the dispersion length modelling for VAS of ammonia/air combustion in porous inert media. Moreover, the relative importance of the individual terms of the gas and solid energy equations of the VAS model for a wide range of dispersion lengths is analysed to highlight the impact of dispersion modelling on the energy budget.

CRediT authorship contribution statement

Rishabh Puri: Conceptualization, Methodology, Investigation, Writing – original draft. **Daniel Kretzler:** Conceptualization, Methodology, Investigation. **Benjamin Bock-Seefeld:** Conceptualization, Methodology, Investigation. **Björn Stelzner:** Conceptualization, Supervision. **Nora Brachhold:** Conceptualization, Supervision. **Jana Hubálková:** Methodology, Investigation. **Dimosthenis Trimis:** Supervision, Project administration, Funding acquisition. **Christos Aneziris:** Supervision, Project administration, Funding acquisition. **Oliver T. Stein:** Supervision, Project administration, Funding acquisition, Writing – review & editing. **Thorsten Zirwes:** Conceptualization, Supervision, Software, Writing – review & editing.

Declaration of competing interest

The authors declare that they have no known competing financial interests or personal relationships that could have appeared to influence the work reported in this paper.

Acknowledgements

The authors are grateful to Dr. Laurent Selle for providing simulation data from CH_4-air combustion in porous media [12]. The authors acknowledge the financial support by DFG, Germany (project number: 523876164, within PP2419 HyCAM) and the Helmholtz Association of German Research Centers (HGF), within the research field Energy, program Materials and Technologies for the Energy Transition (MTET), topic Resource and Energy Efficiency. The authors gratefully acknowledge the Gauss Centre for Supercomputing e.V. (www.gauss-centre.eu) for providing computing time through the John von Neumann Institute for Computing (NIC) on the GCS Supercomputer JURECA at Jülich Supercomputing Centre (JSC).

References

[1] C. Bae, J. Kim, Alternative fuels for internal combustion engines, Proc. Combust. Inst. 36 (3) (2017) 3389–3413.
[2] H. Stančin, H. Mikulčić, X. Wang, N. Duić, A review on alternative fuels in future energy system, Renew. Sustain. Energy Rev. 128 (2020) 109927.
[3] M.D. Allendorf, V. Stavila, J.L. Snider, M. Witman, M.E. Bowden, K. Brooks, B.L. Tran, T. Autrey, Challenges to developing materials for the transport and storage of hydrogen, Nat. Chem. 14 (11) (2022) 1214–1223.
[4] A. Valera-Medina, H. Xiao, M. Owen-Jones, W. David, P. Bowen, Ammonia for power, Prog. Energy Combust. Sci. 69 (2018) 63–102.
[5] A.M. Elbaz, S. Wang, T.F. Guiberti, W.L. Roberts, Review on the recent advances on ammonia combustion from the fundamentals to the applications, Fuel Comm. 10 (2022) 100053.
[6] Q. Cheng, A. Muhammad, O. Kaario, Z. Ahmad, L. Martti, Ammonia as a sustainable fuel: Review and novel strategies, Renew. Sustain. Energy Rev. 207 (2025) 114995.
[7] P. Tamadonfar, S. Karimkashi, T. Zirwes, V. Vuorinen, O. Kaario, A numerical study on premixed laminar ammonia/air flames enriched with hydrogen: An analysis on flame–wall interaction, Combust. Flame 265 (2024) 113444.
[8] H. Nozari, G. Karaca, O. Tuncer, A. Karabeyoglu, Porous medium based burner for efficient and clean combustion of ammonia–hydrogen–air systems, Int. J. Hydrog. Energy 42 (21) (2017) 14775–14785.
[9] G. Vignat, B. Akoush, E.R. Toro, E. Boigné, M. Ihme, Combustion of lean ammonia-hydrogen fuel blends in a porous media burner, Proc. Combust. Inst. 39 (4) (2023) 4195–4204.
[10] J. Lin, X. Li, Y. Zhang, Z. Zhang, S.R. Holden, F. Cheng, D. Zhang, Experimental study on ammonia dissociation and NOx emission under fuel-rich combustion in a porous burner, Combust. Sci. Tech. (2025) 1–17.
[11] A.J. Barra, G. Diepvens, J.L. Ellzey, M.R. Henneke, Numerical study of the effects of material properties on flame stabilization in a porous burner, Combust. Flame 134 (4) (2003) 369–379.
[12] P.-A. Masset, F. Duchaine, A. Pestre, L. Selle, Modelling challenges of volume-averaged combustion in inert porous media, Combust. Flame 251 (2023) 112678.
[13] C. Wieland, C. Weis, P. Habisreuther, D. Trimis, 3D direct pore level simulations of radiant porous burners, Combust. Flame 245 (2022) 112370.
[14] E. Boigné, T. Zirwes, D.Y. Parkinson, G. Vignat, P. Muhunthan, H.S. Barnard, A.A. MacDowell, M. Ihme, Integrated experimental and computational analysis of porous media combustion by combining gas-phase synchrotron μCT, IR-imaging, and pore-resolved simulations, Combust. Flame 259 (2024).
[15] S. Sathe, R. Peck, T. Tong, A numerical analysis of heat transfer and combustion in porous radiant burners, Int. J. Heat Mass Transfer 33 (6) (1990) 1331–1338.
[16] P.-F. Hsu, J.R. Howell, R.D. Matthews, A numerical investigation of premixed combustion within porous inert media, J. Heat Transfer 115 (3) (1993) 744–750.
[17] S. Mishra, M. Steven, S. Nemoda, P. Talukdar, D. Trimis, F. Durst, Heat transfer analysis of a two-dimensional rectangular porous radiant burner, Int. Comm. Heat Mass Trans. 33 (4) (2006) 467–474.
[18] M. Sahraoui, M. Kaviany, Direct simulation vs volume-averaged treatment of adiabatic, premixed flame in a porous medium, Int. J. Heat Mass Transfer 37 (18) (1994) 2817–2834.
[19] M. Bidi, M. Nobari, M.S. Avval, A numerical evaluation of combustion in porous media by EGM (entropy generation minimization), Energy 35 (8) (2010) 3483–3500.
[20] S. Sobhani, S. Allan, P. Muhunthan, E. Boigne, M. Ihme, Additive manufacturing of tailored macroporous ceramic structures for high-temperature applications, Adv. Eng. Mater. 22 (8) (2020) 2000158.
[21] J.C. Ferguson, F. Semeraro, J.M. Thornton, F. Panerai, A. Borner, N.N. Mansour, Update 3.0 to "PuMA: The porous microstructure analysis software", SoftwareX 15 (2021) 100775.
[22] T. Zirwes, G. Vignat, E.R. Toro, E. Boigné, K. Younes, D. Trimis, M. Ihme, Improving volume-averaged simulations of matrix-stabilized combustion through direct X-ray μ CT characterization: Application to NH3/H2-air combustion, Combust. Flame 257 (2023) 113020.
[23] D.G. Goodwin, H.K. Moffat, I. Schoegl, R.L. Speth, B.W. Weber, Cantera: An object-oriented software toolkit for chemical kinetics, thermodynamics, and transport processes, 2023, Version 3.0.0.
[24] M.R. Henneke, J.L. Ellzey, Modeling of filtration combustion in a packed bed, Combust. Flame 117 (4) (1999) 832–840.
[25] P. Parthasarathy, P. Habisreuther, N. Zarzalis, Evaluation of longitudinal dispersion coefficient in open-cell foams using transient direct pore level simulation, Chem. Eng. Sci. 90 (2013) 242–249.
[26] C. Bedoya, I. Dinkov, P. Habisreuther, N. Zarzalis, H. Bockhorn, P. Parthasarathy, Experimental study, 1D volume-averaged calculations and 3D direct pore level simulations of the flame stabilization in porous inert media at elevated pressure, Combust. Flame 162 (10) (2015) 3740–3754.
[27] S.-Y. Hsu, The effects of tortuosity and dispersion on porous combustion, Combust. Theory Model. 25 (7) (2021) 1175–1194.
[28] T. Zirwes, M. Sontheimer, F. Zhang, A. Abdelsamie, F.E.H. Pérez, O.T. Stein, H.G. Im, A. Kronenburg, H. Bockhorn, Assessment of numerical accuracy and parallel performance of OpenFOAM and its reacting flow extension EBIdnsFoam, Flow, Turbul. Combust. 111 (2) (2023) 567–602.
[29] S. Whitaker, Flow in porous media I: A theoretical derivation of Darcy's law, Transp. Porous Media 1 (1) (1986) 3–25.
[30] F. Demaria, R.R. White, Transient response study of gas flowing through irrigated packing, AIChE J. 6 (3) (1960) 473–481, Cited by: 46.
[31] T. Zirwes, A. Kronenburg, Assessment of approximate soret diffusion models for hydrogen and ammonia combustion, Flow, Turbul. Combust. (2025).
[32] G. Brenner, K. Pickenäcker, O. Pickenäcker, D. Trimis, K. Wawrzinek, T. Weber, Numerical and experimental investigation of matrix-stabilized methane/air combustion in porous inert media, Combust. Flame 123 (1) (2000) 201–213.
[33] J. Li, Z. Zhao, A. Kazakov, F.L. Dryer, An updated comprehensive kinetic model of hydrogen combustion, Int. J. Chem. Kinet. 36 (2004) 566–575.
[34] P.-A. Masset, Modelling Challenges of Stationary Combustion in Inert Porous Media (Ph.D. thesis), Institut National Polytechnique de Toulouse - INPT, 2022.
[35] E. Ranzi, A. Frassoldati, A. Stagni, M. Pelucchi, A. Cuoci, T. Faravelli, Reduced kinetic schemes of complex reaction systems: Fossil and biomass-derived transportation fuels, Int. J. Chem. Kinet. 46 (9) (2014) 512–542.
[36] N. Otsu, A threshold selection method from gray-level histograms, IEEE Trans. Syst. Man Cybern. 9 (1) (1979) 62–66.
[37] A. Stagni, C. Cavallotti, S. Arunthanayothin, Y. Song, O. Herbinet, F. Battin-Leclerc, T. Faravelli, An experimental, theoretical and kinetic-modeling study of the gas-phase oxidation of ammonia, React. Chem. Eng. 5 (2020) 696–711.